A Preliminary Approach to Modeling Gas Hydrate/Ice Deposition from Dissolved Water in a Liquid Condensate System

Joseph W. Nicholas, Carolyn A. Koh, and E. Dendy Sloan
Chemical Engineering Dept., Colorado School of Mines, Golden, CO 80401

DOI 10.1002/aic.11921
Published online June 4, 2009 in Wiley InterScience (www.interscience.wiley.com).

Gas hydrate/ice deposition from a dissolved water phase in a liquid condensate system was modeled using a mass and energy balance. The same modeling parameters were used to model three flow loop experiments (1.89 and 2.83 L/min flow rate deposition tests and a 1.89 L/min dissociation test) with acceptable accuracy. Relative changes in both temperature and pressure drop were modeled using an ice deposit with a 67% void fraction. © 2009 American Institute of Chemical Engineers *AIChE J,* 55: 1889–1897, 2009
Keywords: hydrate, ice, deposition, plugging, dissolved water

Introduction

Clathrate hydrates (or gas hydrates) have been known to hinder the oil and gas industry since 1934, when Hammerschmidt discovered hydrates were capable of plugging pipelines.[1] Clathrate hydrates are crystalline inclusion compounds wherein hydrogen-bonded water molecules form cages containing guest molecules.[2] Hydrates form at high pressures and low temperatures, similar to conditions on the seafloor. Offshore pipelines transport hydrocarbon molecules (e.g., methane, ethane, and propane) that can act as hydrate guests and are prime candidates for hydrate formation and plugging. In addition to lost production and revenue, hydrates pose a significant safety hazard, because of gas expansion upon heating and projectile-like properties when dislodged.[3]

In 1994, Lingelem et al.[4] suggested that hydrates formed from gas condensate deposit on the pipe wall, similar to a freezing water pipelne. Recent hydrate field studies conducted in both the Werner Bolley[5] and Tommeliten Gamma[6] fields suggest that hydrates may have adhered to the pipe wall. Both tests observed pressure buildups and falloffs that would be consistent with hydrate deposits on the pipe wall before sloughing downstream to form a plug.

Correspondence concerning this article should be addressed to J. W. Nicholas at joe.nicholas@meritenergy.com or E. D. Sloan at esloan@mines.edu.
Current address of J. W. Nicholas, Merit Energy, 13727 Noel Road, Suite 500, Dallas, TX 75240.

Recently, Nicholas[7] used a single pass flow loop to investigate hydrate/ice deposition in a water saturated liquid condensate system. These flow loop experiments determined that hydrate formation from a dissolved water phase resulted in a lengthwise, uniform/dispersed deposit, which resulted in a gradual pressure drop increase over several days (Nicholas et al., submitted). Similar to wax and frost deposition experiments, the hydrate/ice deposit functioned as an insulator on the pipe wall.[8–14] This resulted in an increase in condensate temperature at the deposit site, forcing dissolved water to deposit as hydrate/ice further downstream in the flow loop.

The prediction of hydrate formation and deposition in water saturated systems is directly applicable to gas export and sales pipelines. Before entering these lines, gas is usually dehydrated to field specifications, occasionally at very low temperatures and very high pressures, these concentration specifications are within hydrate formation conditions.[15] This scenario becomes exacerbated when flowline conditions have fluctuating ambient temperatures, which is the case in many onshore pipelines. Gas export and sales lines affected by seasonal temperatures include: arctic pipelines, residential pipelines, and other lines exposed to harsh winters. A predictive model would allow energy companies to identify the consequences of operating slightly inside the hydrate formation region, which may occur during a seasonal cool down or a dehydrator malfunction.

Table 1. Comparison of Experimental and Predicted Pressure Drop in the Test Section

Distance (m)	Actual ΔP (kPa)	Calculated ΔP (kPa)
0	0	0
12.2	11.7	9.0
24.4	17.9	17.9
36.6	26.9	26.9
48.8	37.9	36.5
61.0	42.7	44.8
73.2	53.1	53.7

Modeling Approach

Nicholas[7] deposited hydrate/ice in a flow loop test section that was 85.3 m (Nicholas et al., submitted). The flow loop was constructed using a series of 6.1 m long, coiled, pipe-in-pipe heat exchangers with an inner diameter of 9.3 mm. Pressure and temperature profiles were measured every minute between each of the 12.2 m sections. Two deposition experiments were completed at 252.5 K using target flow rates of 1.89 (~0.3 m/s) and 2.83 L/min (~0.6 m/s), which were chosen because of pump limitations. A final dissociation experiment was also completed at the end of the 1.89 L/min experiment by passing the inlet stream through a molecular sieve unit[7] (Nicholas et al., submitted).

Matching initial flow loop pressure drop and temperature profiles

Before modeling solid deposition/wall growth, it was imperative to match the test section pressure drop and temperature profiles in the absence of solid deposits. Because the experiment conducted at 2.83 L/min had fewer experimental uncertainties than the lower flow rate experiment, it was chosen as the first system to model. Pressure drop was calculated using a steady-state momentum balance and neglecting gravitational effects[16]

$$\Delta p = 2 f_F \rho \dot{m}^2 \frac{\Delta z}{D} \tag{1}$$

where Δp is pressure drop (Pa), f_F is the Fanning friction factor, ρ is the fluid density (kg/m^3), Δz is the axial distance (m), $\dot{m}$ is the mass flow rate (kg/s), and D is the inner diameter of the flow loop (9.3E-3 m). The Fanning friction factor was fit to match the flow loop pressure drop as shown in Table 1.

The pressure drop calculations shown in Table 1 were completed using a f_F value of 1.07E-2. This value was 18% greater than the predicted factory value of 9.1E-3. However, because the pressure drop calculation did not incorporate the tee connections used for the pressure and temperature transducers (every 12.2 m) or the 14 unions used in coupling the 14 heat exchangers, the fitted value was considered reasonable.

The temperature profile was calculated using an energy balance (Eq. 2), assuming the cooling fluid was maintained at a constant temperature of 252.5 K. This assumption was made because cooling fluid was supplied in parallel to each of the 14 heat exchangers along the flow loop.

$$T_{out} = T_{in} - \frac{q_r}{C_p \dot{m}} \tag{2}$$

T_{in} and T_{out} are the temperature (K) of the fluid entering and exiting the control volume, q_r is the energy (W) transferred from the condensate to the cooling fluid, and C_p is the condensate specific heat capacity (J/kg K). A series of convective resistances (neglecting conduction through the pipe wall) were used to calculate q_r as illustrated in Figure 1.

Figure 1 shows the heat transfer through the pipe wall as a function of: T_B the bulk condensate temperature (K), T_c the cooling fluid temperature (K), r_w the inner radius (m) of the flow loop, r_c the outer radius (m) of the flow loop, h_B the internal heat transfer coefficient (W/m^2 K), and h_c the external heat transfer coefficient (W/m^2 K). The internal heat transfer coefficient, h_B, was calculated using the Chilton–Colburn analogy[17]

$$Nu_D = 0.023\, Re_D^{4/5} Pr^{1/3} = \frac{h_B D}{k} \tag{3}$$

where Nu_D is the Nusselt number, Re_D is the Reynolds number, Pr is the Prandtl number, and k is the thermal conductivity of condensate (with properties assumed to be *n*-decane at 252 K and 1000 psi—0.14 W/m K).[18]

Equation 2 was used to match the bare pipe temperature profile, as shown in Table 2, by fitting h_c to 360 W/m^2 K.

Hydrate/ice deposition model

Hydrate/ice was modeled using a simplified version of the wax deposition model presented by Singh et al.[8] The modeled geometry is shown in Figure 2. The subscript i in Figure 2 denotes the radius, temperature, and concentration profiles at the condensate-solid interface. Several assumptions were used in modeling the flow loop data:

(1) Water concentration at the solid–liquid condensate (solid-L_{cond}) interface was in equilibrium with the interface temperature.

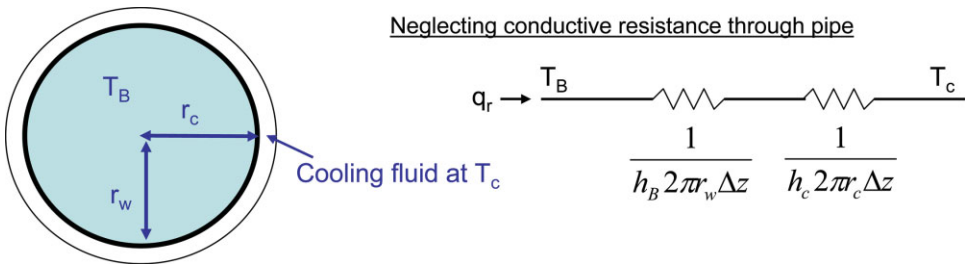

Figure 1. Schematic of pipe-in-pipe flow loop configuration and the internal and external convective resistances in series with each other.

[Color figure can be viewed in the online issue, which is available at www.interscience.wiley.com.]

Table 2. Comparison of Experimental and Calculated Temperature Profiles

Distance (m)	Actual Temp (K)	Calculated Temp (K)
0	287.5	287.5
12.2	258.9	258.7
24.4	254.2	253.6
36.6	252.6	252.6

(2) Hydrate/ice was assumed to be deposited uniformly, with respect to radius and distance, in each Δz increment.

(3) Heat transfer was assumed to be one dimensional (radial) and quasi-steady state.

(4) Hydrate/ice was assumed to be of constant density. The present model does not incorporate the "aging" mechanism discussed in Singh et al.'s work.[8] Because density, thickness, and morphology were not directly measured in the flow loop experiments, the accuracy of an aging model could not be tested. Thus, constant density was assumed to reduce computational complexity.

Change in hydrate/ice thickness was calculated using the following mass balance on the water phase

$$\begin{gathered}\text{In} - \cancel{\text{Out}} + \cancel{\text{Gen}} = \text{Accumulation} \\ 2\pi\Delta z r_i h_m [C_B - C_i(T_i)] = \frac{d}{dt}[\pi\Delta z(r_w^2 - r_i^2)\rho_s]\end{gathered} \tag{4}$$

where ρ_s is the density of the solid deposit (kg/m^3), r_i is the radius of the solid front (m), and h_m is the mass transfer coefficient (m/s). The mass transfer coefficient was calculated in an analogous manner to the heat transfer coefficient

$$\text{Sh}_D = 0.023\,\text{Re}_D^{4/5}\text{Sc}^{1/3} = \frac{h_m D}{D_{WC}} \tag{5}$$

where Sh_D is the Sherwood number, Sc is the Schmidt number, and D_{wc} is the molecular diffusion coefficient of water in condensate. D_{wc} (cm^2/s) was calculated using the Wilke–Chang correlation[19]

$$D_{wc} = \left(\frac{7.4 \times 10^{-8}(\phi_c M_c)^{1/2} T}{\mu_c v_w^{0.6}}\right) \tag{6}$$

where ϕ_c is the association factor of the condensate (chosen to be 1 because of the range of components in the condensate, [Nicholas et al., submitted][20]), M_c is the molecular weight of the condensate (142 g/mol), T is the temperature (273 K), μ_c is the viscosity of the condensate (0.264 cP), and v_w is the molar volume of water (18 cm^3/mol). Equation 6 yields a predicted diffusion coefficient for water in condensate of 1.6E-4 cm^2/s.

The two unknowns in Eq. 4 are r_i and T_i. T_i was calculated using an energy balance across the control volume, assuming that heat transfer occurred instantaneously and the deposit did not accumulate energy. Thus, quasi-steady state was assumed for energy accumulation

$$\begin{gathered}\text{In} - \text{Out} + \text{Generation} = \text{Accumulation} \\ 2\pi\Delta z r_i h_B (T - T_i) - 2\pi\Delta z r_i u'[T_i - T_c] \\ + 2\pi\Delta z r_i h_m [C_B - C_i(T_i)]\Delta H_f = 0\end{gathered} \tag{7}$$

where ΔH_f is the latent heat of solid formation. The value u' is the combined heat transfer coefficient, incorporating solid thermal conductivity and the external heat transfer coefficient in series

$$u' = \frac{1}{\frac{\ln\left(r_w/r_i\right)}{k_s} + \frac{1}{h_c r_c}} \tag{8}$$

where k_s is the thermal conductivity of the composite solid deposit (W/m K).

The flow loop was divided into sections (Δz) as illustrated in Figure 3. In each section, Eq. 7 was used to solve for the interface temperature, T_i. The interface temperature was then used to calculate the equilibrium water concentration at the solid interface. This allowed the change in radius, r_i, to be calculated with Eq. 4. Energy and mass balances were then conducted on the exiting fluid and the process was repeated in the next section of pipe. After solving Eqs. 4 and 7 for the entire flow loop, the model moved to the next time step and restarted at the flow loop inlet. It is important to note that the variables changing with diameter, such as h_B and h_m, were recalculated at each distance and time step.

After calculating the thickness profiles of the solid deposits from Eq. 4, pressure drop was calculated to compare with experimental data. Equation 1 was used to calculate pressure drop for each Δz using the effective radius of the solid deposit and assuming mass flow rate remained constant. The pressure drop calculations were then summed over the entire

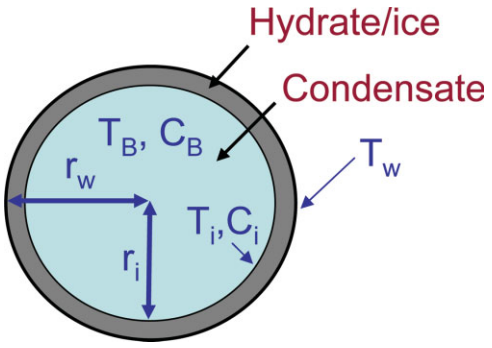

Figure 2. Schematic of pipe wall, hydrate/ice deposit, and the corresponding temperatures (T_x) and concentrations (C_x) tracked in the transport model.

Subscript "i" is the interface, "B" is the bulk, and "w" is the wall. [Color figure can be viewed in the online issue, which is available at www.interscience.wiley.com.]

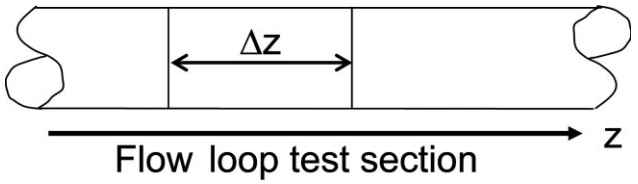

Figure 3. Illustration of the flow loop, which was divided into sections in the model.

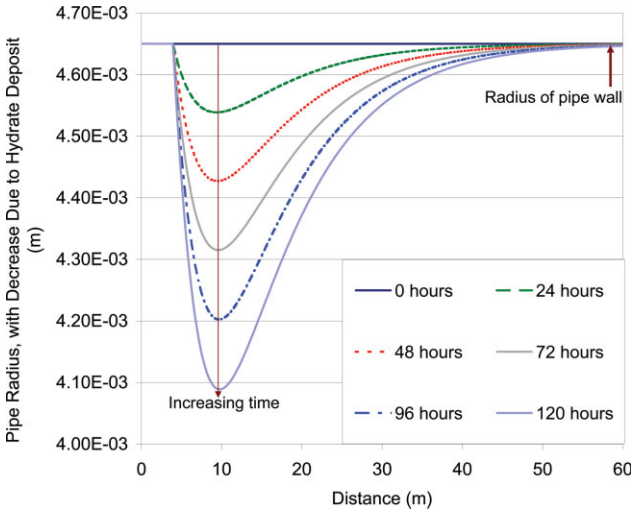

Figure 4. Predicted hydrate radii from 0 to 120 h, through the first 60 m of the flow loop test section using pure hydrate for the 2.83 L/min test.

[Color figure can be viewed in the online issue, which is available at www.interscience.wiley.com.]

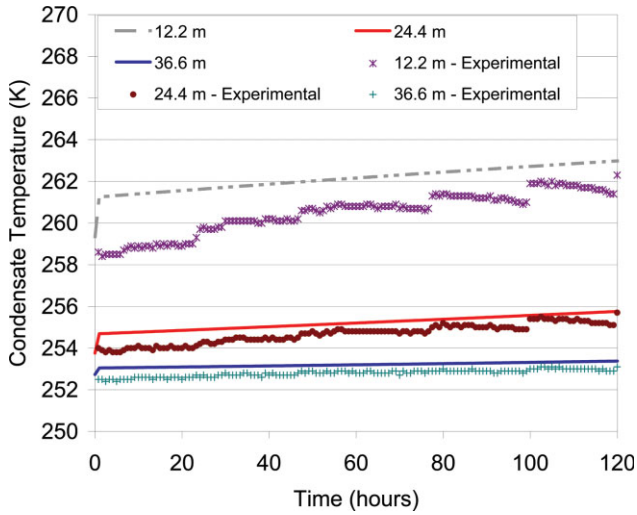

Figure 5. Experimental and predicted temperature profiles assuming pure hydrate at 2.83 L/min.

[Color figure can be viewed in the online issue, which is available at www.interscience.wiley.com.]

test section. Because the hydrate deposit was expected to increase the surface roughness of the pipe wall, the greater of two values was used as the friction factor: (1) the value used for fitting the bare pipe, or (2) the friction factor calculated using the explicit form of the Colebrook and White correlation. The Colebrook and White correlation calculates the friction factor as a function of surface roughness[16,21]

$$f_F = \left\{ -1.737 \ln\left[0.269\frac{\varepsilon}{D} - \frac{2.185}{\mathrm{Re}} \ln\left(0.269\frac{\varepsilon}{D} + \frac{14.5}{\mathrm{Re}} \right) \right] \right\}^{-2} \tag{9}$$

where ε represents the surface roughness. This work assumes that the deposit was rough and the average hydrate thickness ($r_w - r_i$) was equal to ε.

Modeling Results and Discussion

Flow loop experiments were modeled assuming that the inlet concentration was 25 ppmw and the cooling fluid temperature (T_c) was constant at 252 K. A curve was fit to the predicted equilibrium points allowing equilibrium water concentrations at the interface (C_i) to be predicted after calculating the interface temperature (Eq. 7).[22] A forward marching explicit algorithm was used with time and distance steps set to 120 s and 0.1 m, respectively. To ensure the model used sufficiently small time and distance steps, the model was also run using increased time and distance steps of 240 s and 0.2 m. The average difference between the base case runs and runs completed with increased distance/time steps was less than 0.5%.[7]

Hydrate base case and sensitivity analysis

The 2.83 L/min test was initially modeled using properties for pure structure II hydrate ($k_s = 0.5$ W/m K, $\rho_s = 900$ kg/m^3).[2] The predicted hydrate deposit, formed from the dissolved water phase, qualitatively matched the experimental trends observed by Nicholas et al. (submitted). The initial radius at 0 h is the original pipe radius of 4.65E-3 m. The hydrate thickness increased with time, which is observed by the decreasing hydrate radius in Figure 4. Another encouraging aspect of Figure 4 is that the hydrate growth propagates downstream with time, similar to the observed experimental pressure drop trend. This behavior is explained by the increased heat transfer resistance due to hydrate deposition, as shown by the temperature profiles in Figure 5.

Figure 5 shows the temperature profiles at varying distances in the test section. It is important to note that the step changes in the experimental temperature profiles resulted from increasing the pump speed. As the deposit increased,

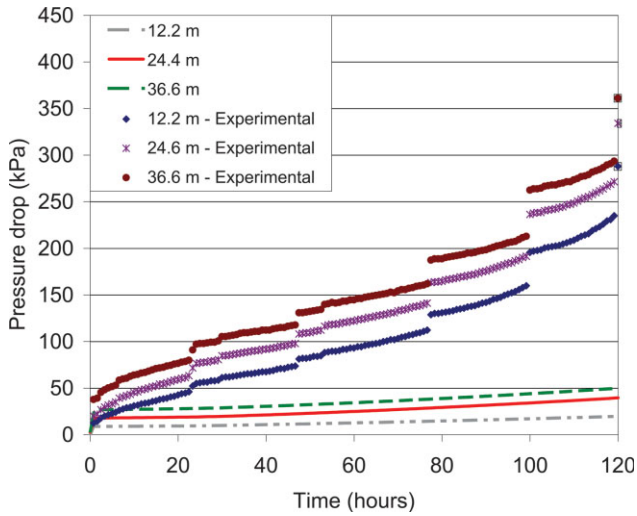

Figure 6. Experimental and predicted pressure drop assuming pure hydrate at 2.83 L/min.

[Color figure can be viewed in the online issue, which is available at www.interscience.wiley.com.]

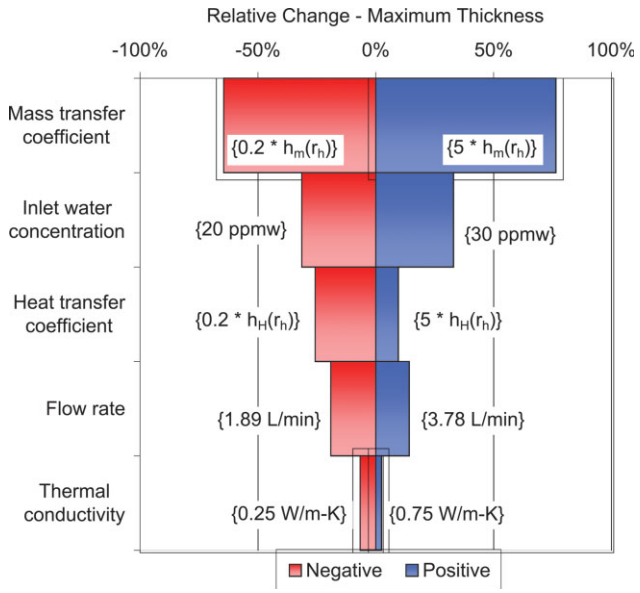

Figure 7. Tornado diagram summarizing the sensitivity analysis on the maximum hydrate thickness using pure hydrate and a 2.83 L/min flow rate as the base case.

[Color figure can be viewed in the online issue, which is available at www.interscience.wiley.com.]

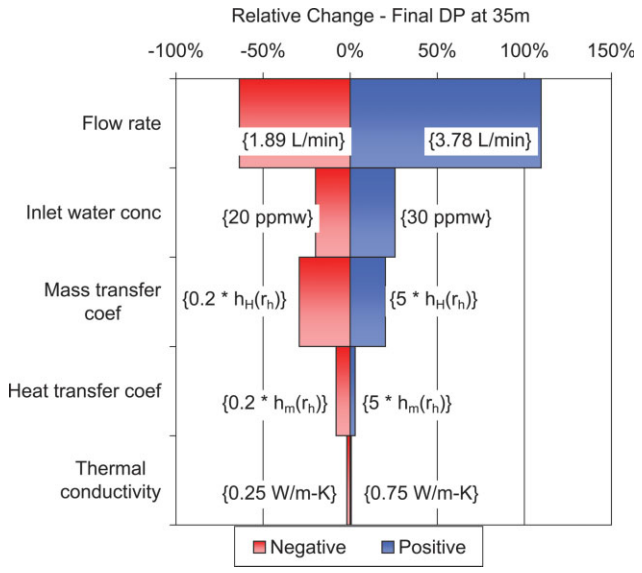

Figure 8. Tornado diagram summarizing sensitivity analysis on the final pressure drop at 35 m, using pure hydrate and a flow rate of 2.83 L/min as a base case.

[Color figure can be viewed in the online issue, which is available at www.interscience.wiley.com.]

the loop pressure drop also increased, resulting in a decreasing flow rate at a constant pump speed. Thus, the pump speed was manually increased to maintain a constant flow rate, as pressure drop increased with solid deposition. Because the temperatures at a given point in the flow loop increased with an increase in flowrate, the temperature profiles should be compared directly after the increase in pump speed (signified by the step change in temperature).[7] Figure 5 shows that the predicted temperature profiles match the measured temperature increase at corresponding locations.

The final piece of information for comparing experimental data and predicted results was the pressure drop shown in Figure 6. Figure 6 shows that the calculated pressure drop profiles under predict the experimental pressure drop. Equation 1 shows that the pressure drop was likely to be underpredicted because of errors in the friction factor or the hydrate thickness. Comparing Eq. 1 and Figure 6 shows the friction factor would have to be multiplied by a factor of 5 to match the final experimental pressure drop. The current model assumption that the hydrate thickness is equal to pipe surface roughness in Eq. 9 is expected to yield an upper limit on the friction value and should not require an increase by a factor of 5. The friction factor was unlikely to explain the difference between experimental and predicted pressure drops in Figure 6.

A sensitivity analysis was conducted to further investigate sources of error related to experiments and transport correlations. Parameters investigated in the sensitivity analysis were as follows: the heat transfer coefficient (internal), mass transfer coefficient, inlet water concentration, and flow rate. The range of values tested was expected to encompass the range of error that may have been present in each variable. The results of this sensitivity analysis are shown in Figures 7 and 8.

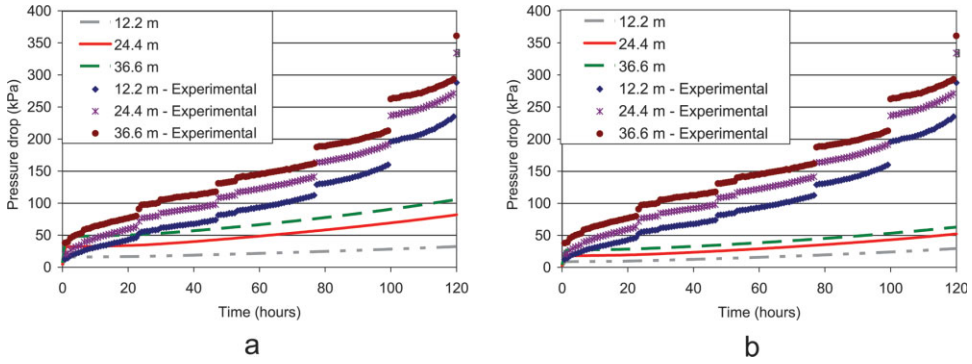

Figure 9. Comparison of predicted and experimental pressure drop using pure hydrate (a) with a flow rate of 3.78 L/min and (b) with an inlet concentration of 30 ppmw.

[Color figure can be viewed in the online issue, which is available at www.interscience.wiley.com.]

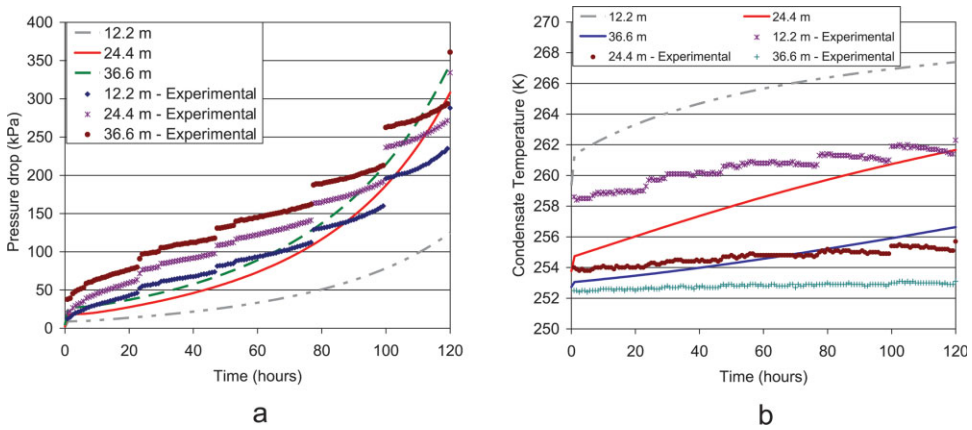

Figure 10. Comparison of 2.83 L/min flow rate predicted and experimental values using hydrate with a 73% void fraction (a) pressure drop profiles and (b) temperature profiles.

[Color figure can be viewed in the online issue, which is available at www.interscience.wiley.com.]

Figures 7 and 8 show how adjusting each variable affects the maximum hydrate thickness and pressure drop, respectively. Because the majority of the deposition behavior occurred within the first 35 m, this distance was chosen as the point of comparison for the calculated pressure drop. The center line represents the base case thickness/pressure drop and the relative change is shown for the range of values tested. The experimental error of water concentration and flow rate was expected to between ±5 ppmw and ±0.95 L/min, respectively. The estimated uncertainty surrounding the heat and mass transfer coefficients was ±5× and the thermal conductivity of hydrate was adjusted ±0.25 (W/m K). Figure 7 shows that the mass transfer coefficient and inlet water concentration had the greatest affect on the maximum thickness. However, the largest change in pressure drop was associated with flow rate and the inlet water concentration.

The pressure drop profiles for the 3.78 L/min flow rate and 30 ppmw inlet concentration are shown in Figure 9. This figure shows the high flow rate and inlet water concentration still significantly under predicted pressure drop. Given the results of this sensitivity analysis, it was apparent that another factor needed to be included in the model.

Porous hydrate and ice deposits

The previous section explored a wide range of variables, yet the pressure drop was under predicted in each circumstance. Revisiting Eq. 1 reveals that the pressure drop is inversely proportional to D.[5] This suggests that the experimental deposit must have been thicker than the predicted deposits, which could be explained by porous deposits. Both the frost and wax literature describe an initially porous deposit that anneals with time.[8,10–14] It is hypothesized that this effect is true of hydrate/ice deposits as well. The effect of porosity was tested by assuming the hydrate deposit had a void fraction of 73%. The composite thermal conductivity was calculated using a volumetric average of the hydrate and condensate fractions.

Figure 10 shows that the final pressure drop was matched to the same order of magnitude as the experimental data. However, the predicted temperature profiles significantly over predicted the data. A possible explanation for the temperature divergence in Figure 10b is that the composite thermal conductivity was too low. The difference in predicted equilibrium water concentrations between ice and hydrate is ~2 ppmw at 252 K.[7,22] Given the uncertainty in formation

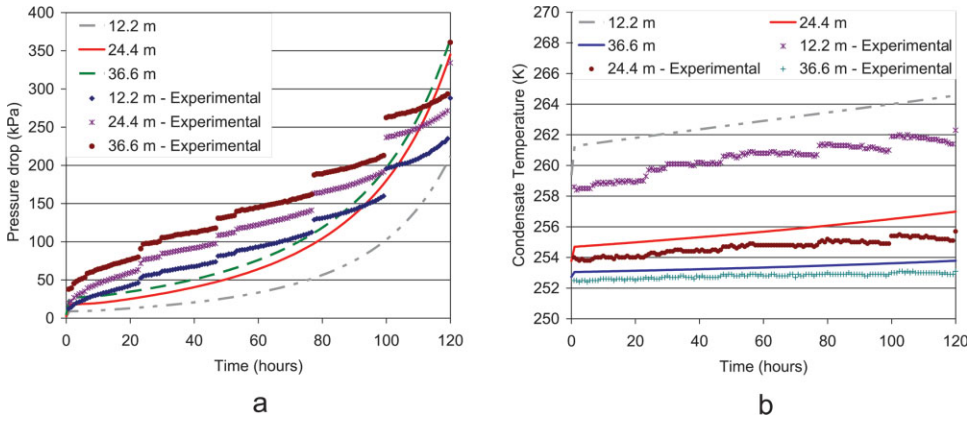

Figure 11. Comparison of 2.83 L/min flow rate predicted and experimental values using ice with a void fraction of 67% (a) pressure drop profiles and (b) temperature profiles.

[Color figure can be viewed in the online issue, which is available at www.interscience.wiley.com.]

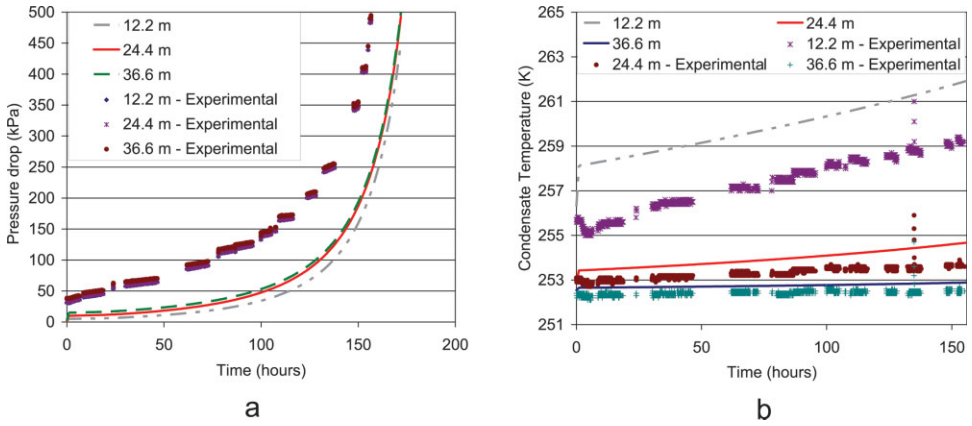

Figure 12. Comparison of 1.89 L/min predicted and experimental values using an ice void fraction of 67% (a) pressure drop profiles and (b) temperature profiles.

[Color figure can be viewed in the online issue, which is available at www.interscience.wiley.com.]

kinetics at that temperature, it is possible that the deposit was metastable ice, rather than hydrate. This is significant because ice has a thermal conductivity of 2.23 W/m K or approximately four times the value used for hydrate.[2]

The results of modeling the flow loop deposit as a porous (67%) ice deposit are shown in Figure 11. Similar to the porous hydrate deposit, pressure drop was matched to the same order of magnitude. However, the temperature profiles of the porous ice deposit exhibited a much closer match to the experimental data. It should be noted that the ice deposit required a less porous deposit than the hydrate deposit to match pressure drop. This is due to the increased thermal conductivity of the ice deposit, which resulted in a more localized deposit than the hydrate.

Figure 11a shows that the pressure drop profiles are still under predicted in the initial stages of the experiment. This can be attributed to the use of a constant density in the model. It is likely that the deposit was initially more porous than the 67% void fraction and then annealed to that average value as the experiment progressed.

Modeling 1.89 L/min flow rate

After fitting the 2.83 L/min data, the 1.89 L/min data set was investigated. It is important to note that there was a major disruption (leak) in the middle of this experiment, which was removed from the data set. Similar to 2.83 L/min data, the friction factor and external heat transfer coefficient were fit to the bare pipe and were determined to be 0.0134 and 328 W/m^2 K, respectively. The flow rate was decreased from 2.83 to 1.89 L/min and the remaining parameters were identical to those used in Figure 11.

It was encouraging that the porous ice deposit (67% void fraction) used in the 2.83 L/min experiment reasonably predicted the 1.89 L/min temperature and pressure drop profiles. Figure 12 shows that the predicted pressure drop and temperature profiles qualitatively match the experimental data.

The 1.89 L/min predicted pressure drop profile is slightly delayed compared with the experimental data. Possible explanations for this difference are the experimental procedure and the previously mentioned disruption in the middle of the experiment.[7] Before conducting this long-term deposition experiment, an unknown amount of hydrate/ice was deposited in the test section. Thus, the model is expected to under predict the total volume of hydrate in the flow loop and under predict the pressure drop as shown in the first 120 h of the comparison.

The final portion of experimental data to be modeled was the 1.89 L/min dissociation. Experimentally, a dehydrator was placed in-line with condensate flow, effectively lowering the inlet water concentration to a value of 3 $\pm$ 1 ppmw.[7] The undersaturated stream then dissociated the deposit. Dissociation was modeled with the same model used in the deposition, except the inlet concentration was reduced from 25 to 3 ppmw. The initial ice thickness profile was equivalent to the final predicted deposit profile used to calculate pressure drop in Figure 12. Figure 13 shows the ice thickness

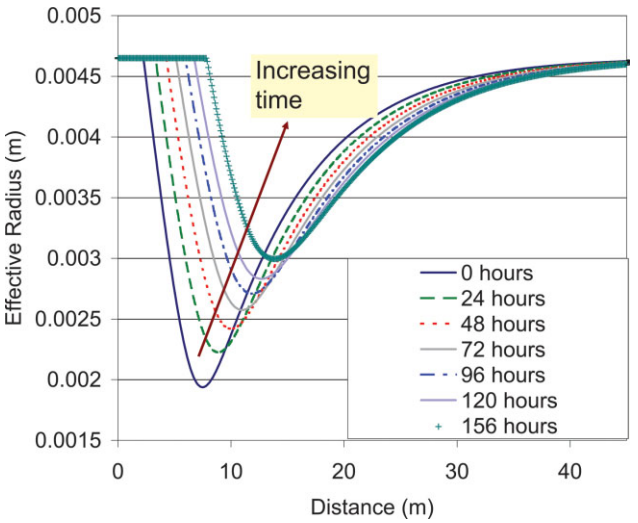

Figure 13. Predicted deposit profile during dehydration portion of the 1.89 L/min experiment.

[Color figure can be viewed in the online issue, which is available at www.interscience.wiley.com.]

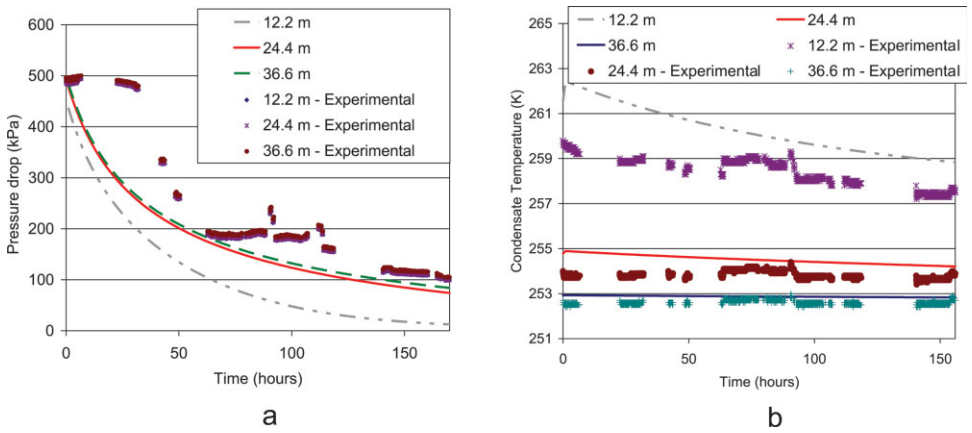

Figure 14. Comparison of predicted and experimental values during 1.89 L/min dehydration (a) pressure drop profiles and (b) temperature profiles.

[Color figure can be viewed in the online issue, which is available at www.interscience.wiley.com.]

decreased with time and slowly propagated downstream. This is consistent with the experimental observation that the undersaturated condensate dissociated the hydrate/ice deposit in the warm upstream portions of the test section; before redepositing the water as hydrate/ice as the condensate flowed downstream and was cooled.

Figure 14a shows the predicted pressure drop decreases and matches the final experimental pressure drop. Likewise, the temperature profile (Figure 14b) shows the predicted temperature profile matches the relative change observed in the experiment. However, upon further examination, the predicted pressure drop profile does not match the initial time delay before pressure drop began to decrease. It was determined that this behavior could be matched by adjusting the diffusion coefficient (D_{wc}), which was proportional to the mass transfer coefficient.

Figure 15 probes the effect of the diffusion coefficient on the pressure drop profiles. It can be observed that increasing the predicted value of D_{wc} (1.6E-8 m^2/s) by a factor of 2 or 2.5, yields a closer match between the predicted and experimental pressure drops. Two possible explanations for this behavior are (1) an incorrect value of D_{wc} (or association factor in Eq. 6) was used, or (2) portions of the deposit were sheared off the wall and rapidly dissolved in the condensate as the deposit dissociated.

Conclusions

Hydrate/ice deposition from a dissolved water phase in a liquid condensate system was modeled using a mass and energy balance. The same modeling parameters were used to model three experiments (1.89 and 2.83 L/min flow rate deposition tests and 1.89 L/min dissociation test), matching the qualitative and quantitative pressure drop and temperature behaviors as show in Figures 11, 13, and 14. The models used an ice deposit with a 67% void fraction, and dissociation was successfully modeled by decreasing the inlet concentration in the deposition model.

The comparison of the model and experimental data suggests that the deposit annealed (became denser) with time, as observed in both frost and wax literature. However, additional experiments capable of measuring the actual thickness

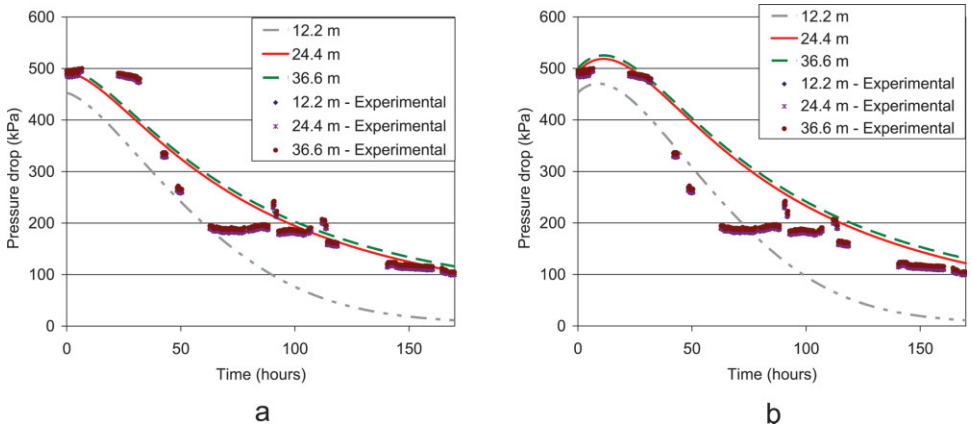

Figure 15. Comparison of predicted and experimental pressure drop profiles for 1.89 L/min dehydration test (a) increasing D_{wc} by 2× and (b) increasing D_{wc} by 2.5×.

[Color figure can be viewed in the online issue, which is available at www.interscience.wiley.com.]

and density of the deposits are required to further refine the current model.

Notation

C_p = heat capacity of condensate (J/kg K).
D = inner diameter of pipe/deposit (m).
D_{wc} = diffusion coefficient of water in condensate (cm^2/s or m^2/s).
f_F = Fanning friction factor.
h_B = internal/bulk heat transfer coefficient (W/m^2 K).
h_c = external heat transfer coefficient (W/m^2 K).
h_m = mass transfer coefficient (m/s).
k = thermal conductivity of deposit (W/m).
$\dot{m}$ = mass flow rate (kg/s).
M_c = molecular weight of condensate (g/mol).
Nu_D = Nusselt number.
Pr = Prandtl number.
q_r = radial heat transfer (W).
r_i = radius of solid interface (m).
r_w = radius of the wall (m).
Re_D = Reynolds number.
Sc = Schmidt number.
Sh_D = Sherwood number.
T_{in} = condensate temp entering Δz (K).
T_{out} = condensate temp leaving Δz (K).
v_w = molar volume of water (cm^3/mol).
ε = surface roughness (m).
Δp = pressure drop (Pa or kPa).
Δz = axial distance step.
ϕ_c = association factor.
ρ = density of condensate (kg/m^3).
ρ_s = density of hydrate/ice (kg/m^3).
μ_c = viscosity of condensate (Pa s).

Literature Cited

1. Hammerschmidt EG. Formation of gas hydrates in natural gas transmission lines. *Ind Eng Chem.* 1934;26:851–855.
2. Sloan ED, Koh CA. *Clathrate Hydrates of Natural Gases*, 3rd ed. Boca Raton, FL: Taylor and Francis Group, LLC, 2008.
3. Sloan ED. *Hydrate Engineering*. Texas: Richardson, 2000.
4. Lingelem MN, Majeed AI, Stange E. Industrial experience in evaluation of hydrate formation, inhibition and dissociation in pipeline design and operation. *Ann NY Acad Sci*. 1994;715:75.
5. Hatton GJ, Kruka VR. *Hydrate Blockage Formation—Analysis of Werner Bolley Field Test Data*. DeepStar CTR 5209–1, 2002.
6. Austvik T, Hustvedt E, Meland B, Berge LI, Lysne D. Tommeliten Gamma field hydrate experiments. *7th BHRA International Conference on Multiphase Flow, Pblctn 14, Cnnes, FR 6/7–9/95*, 1995:539.
7. Nicholas JW. *Hydrate Deposition in Water Saturated Liquid Condensate Systems*. Golden: Colorado School of Mines, 2008.
8. Singh P, Venkatesan R, Fogler SH. Formation and aging of incipient thin film Wax-oil gels. *AIChE J*. 2000;46:1059–1074.
9. Hernandez OC, Hensley H, Sarica C, Brill J, Volk M, Delle-Case E. Improvements in single-phase paraffin deposition modeling. *SPE Prod Facil*. 2004;19:237–243.
10. Le Gall R, Grillot JM. Modeling of frost growth and densification. *Int J Heat Mass Transfer*. 1997;40:3177–3187.
11. Lee K-S, Kim W-S, Lee T-H. A one-dimensional model for frost formation on a cold flat surface. *Int J Heat Mass Transfer*. 1997;40:4359–4365.
12. Hayashi Y, Aoki A, Adachi S, Hori K. Study of frost properties correlating with formation types. *J Heat Transfer*. 1977;99:239–245.
13. Mao Y, Besant RW, Rezkallah KS. Measurement and correlations of frost properties with airflow over a flat plate. *ASHRAE Trans*. 1992;98:65–78.
14. Na B, Webb RL. New model for frost growth rate. *Int J Heat Mass Transfer*. 2004;47:925–936.
15. Kane M, Singh A, Hanssen R. Hydrates blockage experience in a deep water subsea dry gas pipeline: lessons learned. *Offshore Technology Conference*, Houston, TX, May 5–8, 2008.
16. Wilkes JO. *Fluid Mechanics for Engineers*. New Jersey: Prentice-Hall PTR, 1999.
17. Incropera FP, Dewitt DP. *Fundamentals of Heat and Mass Transfer*, 4th ed. New York: Wiley, 1996.
18. NIST, Thermophysical Properties of Fluid Systems. Available at: http://webbook.nist.gov/chemistry/fluid/: 2008.
19. Wilke CR, Chang P. Correlation of diffusion coefficients in dilute solutions. *AIChE J*. 1955;1:264–270.
20. Perry RP, Green DW. *Perry's Chemical Engineers Handbook*, 7th ed. New York: McGraw-Hill, 1997.
21. Olujic Z. Compute friction factors fast for flow in pipes. *Chem Eng*. 1981;88:91–94.
22. INFOCHEM*MULTIFLASH, Version 3.7.05*, London, 2007.

Manuscript received Sept. 22, 2008, and revision received Mar. 13, 2009.